Chemical Physics Letters xxx (2011) xxx–xxx

Contents lists available at ScienceDirect

Chemical Physics Letters

journal homepage: www.elsevier.com/locate/cplett

Bonding and vibrations of CH_xO and CH_x species (x = 1–3) on a palladium nanoparticle representing model catalysts

Sergey M. Kozlov [a], Gabriela F. Cabeza [b,*], Konstantin M. Neyman [a,c,*]

[a] Departament de Química Física, Institut de Química Teòrica i Computacional (IQTCUB), Universitat de Barcelona, 08028 Barcelona, Spain
[b] Departamento de Física, Universidad Nacional del Sur, 8000 Bahía Blanca, Argentina
[c] Institució Catalana de Recerca i Estudis Avançats (ICREA), 08010 Barcelona, Spain

ARTICLE INFO

Article history:
Received 5 January 2011
In final form 27 February 2011
Available online xxxx

ABSTRACT

This computational study deals with the adsorption of CH_3, CH_2, CH, CH_2OH, CH_3O, CH_2O and CHO species on a nanoparticle Pd_{79} that mimics experimentally investigated model Pd catalysts. We quantify structural, energetic and vibrational parameters of these adsorption complexes and analyse their dependence on the adsorption site. Most of the considered low coordinated adsorption sites are found to be favoured by 20–50 kJ/mol over the sites on (1 1 1) facets. Some of the studied species have distinguishable vibrational parameters at different adsorption sites of the model nanoparticle, making possible spectroscopic characterization of respective adsorption complexes.

1. Introduction

Recent advances in surface science provided deep insights into the energetics, kinetics and mechanisms of reactions at solid surfaces [1]. Studies on well-defined model surfaces in ultrahigh vacuum also illuminated important details of many processes in heterogeneous catalysis ([2,3] and references therein). However, it is well recognized nowadays that profound understanding of processes on single crystal surfaces cannot be automatically translated into an equally good understanding of heterogeneous catalysis. One of the main reasons for that is a high structural disorder and heterogeneity of the real catalysts vs. the single crystal surfaces, which has been denoted as the 'material gap' [4]. Experimentalists made attempts to bridge this gap quite early, by preparing model catalysts consisting, e.g. of well-characterised metal nanoparticles deposited on metal–oxide films [5,6]. Appropriate high-level computational efforts were notably delayed [7,8].

The simplest organic molecules and radicals with just one carbon atom, e.g. CH_xO and CH_x (x = 1–3), are ubiquitous intermediates and reactants in a variety of important catalytic processes, including chemical transformations of methanol (CH_3OH) [9], methane (CH_4) [10] and other chemicals. The progress in identification of reaction intermediates and catalytically active sites through in situ characterization techniques, including vibrational spectroscopy, has been recently reviewed [11–13] and considerable differences due to catalyst nanostructuring have been documented. Also, first density-functional (DF) computational investigations clearly revealed notable nano-effects for transition and noble metal catalysts with respect to their adsorption properties and reactivity [7,14–20]. So far the DF modeling of the CH_xO and CH_x species interacting with Pd has been mainly limited to single-crystal surfaces ([21] and references therein). The most relevant DF studies [15,16] were related to methanol decomposition on nanocrystalline Pd catalysts and focused on the CH_x intermediates and transition states involved in the slow C–O bond scission path of methoxide. In these studies, localized Gaussian-type basis sets were employed and, due to symmetry restrictions, eight adsorbed species – one per each (1 1 1) facet – had to be accommodated on the model cub-octahedral Pd nanoparticles.

The main goal of the present DF study is to determine and possibly quantify the distinctive characteristics of the adsorption complexes of various above-mentioned C_1 species involved in chemical reactions on Pd catalysts and caused by nano-structuring of the latter. In particular we (i) inspect whether the low-coordinated edge/corner sites of Pd nanoparticles are energetically favourable for the adsorption of the C_1 species and (*ii*) search for the opportunities to spectroscopically characterise the adsorbates and differentiate between locations on the regular terrace and edge/corner sites of the Pd catalysts, for instance, employing differences in the vibrational fingerprints. This information is useful to gain new insights into the mechanisms of a broad spectrum of industrially-relevant reactions on such an indispensable catalytic material as palladium.

2. Computational details and models

Calculations were carried out with the help of the VASP code [22,23], in which Kohn–Sham functions are expanded in a basis

* Corresponding authors. Address: Departament de Química Física and Institut de Química Teòrica i Computacional (IQTCUB), Universitat de Barcelona, 08028 Barcelona, Spain (K.M. Neyman).
E-mail addresses: gcabeza@uns.edu.ar (G.F. Cabeza), konstantin.neyman@icrea.es (K.M. Neyman).

0009-2614/$ - see front matter © 2011 Elsevier B.V. All rights reserved.
doi:10.1016/j.cplett.2011.02.061

of periodic plane waves. The core–valence interaction was treated using the projector augmented wave (PAW) method [24] with the cut-off energy for plane waves of 415 eV. The RPBE [25] form of the Generalized Gradient Approximation (GGA) was employed. The total energy tolerance defining self-consistency of the electron density was 10^{-4} eV. To speed up convergence of the Kohn–Sham self-consistent process, a first-order Methfessel–Paxton smearing of 0.1 eV has been applied and then total energies were extrapolated to 0 K (no smearing). Structures were optimised until the maximum forces acting on each atom became less than 0.01 eV/Å. Only spin-restricted calculations of the adsorption systems have been performed, which are considered accurate enough for the purposes of the present model study [26]. Calculations of the reference gas-phase C_1 species were performed using the spin-polarized approach, which yielded the following ground states: CH – doublet, CH_2 – triplet, CH_3 – doublet, CH_2OH – doublet, CH_3O – doublet, CH_2O – singlet, CHO – doublet. Only the Γ point was used for sampling the Brillouin zone of the discrete nanoparticles.

A cub-octahedral nanoparticle Pd_{79} [7] is a cut out of bulk structure that exhibits only low-index (1 1 1) and (1 0 0) Miller planes on the surface. Its (1 1 1) facets were shown to be in the so-called 'scalable-to-bulk' regime (e.g. [14–17]), i.e. their structural and adsorption properties scale with increasing particle size to those of bulk-like samples [27,28]. However, the (1 0 0) nanofacets of the Pd_{79} particle, consisting of only four atoms, (and their edges) appear to be too small to adequately represent (1 0 0) facets (and edges) of larger metal nanoparticles commonly dealt with in catalytic experiments [5,14]. That is why we deliberately refrained from considering interactions with the sites at the (1 0 0) facets by means of the present model Pd_{79}. The supercell approach is used; the nanoparticle with the adsorbate under scrutiny C_1/Pd_{79} located in a cubic cell $2.4 \times 2.4 \times 2.4$ nm is separated from its images by at least 1 nm. Thus, artificial interactions between periodically repeated images are avoided. Only the lowest-coverage limit with just one C_1 species per Pd_{79} nanoparticle is considered. For brevity, all studied structures for each adsorbate are grouped together in one panel of Figure 1.

While we always fully optimised atomic positions of the adsorbates, three types of models were considered for the Pd_{79} nanoparticle interacting with CH_x (Table 1): **1** – all Pd atoms were kept at the experimental positions as in bulk Pd with r(Pd–Pd) = 275 pm, **2** – all Pd atoms were kept at the RPBE optimised positions of bare Pd_{79} and the optimization was restricted to atoms of the adsorbed CH_x, **3** – Pd_{79} fully optimised together with the adsorbates. Optimization of bare Pd_{79} with the gradient-corrected RPBE functional and PAW technique to treat core electrons yields a somewhat rounded structure [7,26,29], which exhibits on its (1 1 1) nanofacets Pd–Pd distances from 272 pm (between atoms on the long edges) to 277 pm (between Pd atoms on the edges and on the terrace), notably shorter than the bulk-optimised Pd–Pd distance of 282 pm. Only the approach **2** has been used for the CH_xO/Pd_{79} complexes. According to vibrational analysis, all calculated structures (except CH_2 adsorbed at site **A**, see below) represented local minima on the potential energy surface. Harmonic vibrational frequencies (for the anharmonicity corrections of the free C_1 species addressed here we refer to [30]) were calculated with the finite difference method, in which Hessian matrix was obtained by displacing all atoms of the adsorbates by ±2 pm from the equilibrium positions in all three Cartesian directions. We illustrate the accuracy of the RPBE calculated harmonic vibrational frequencies for

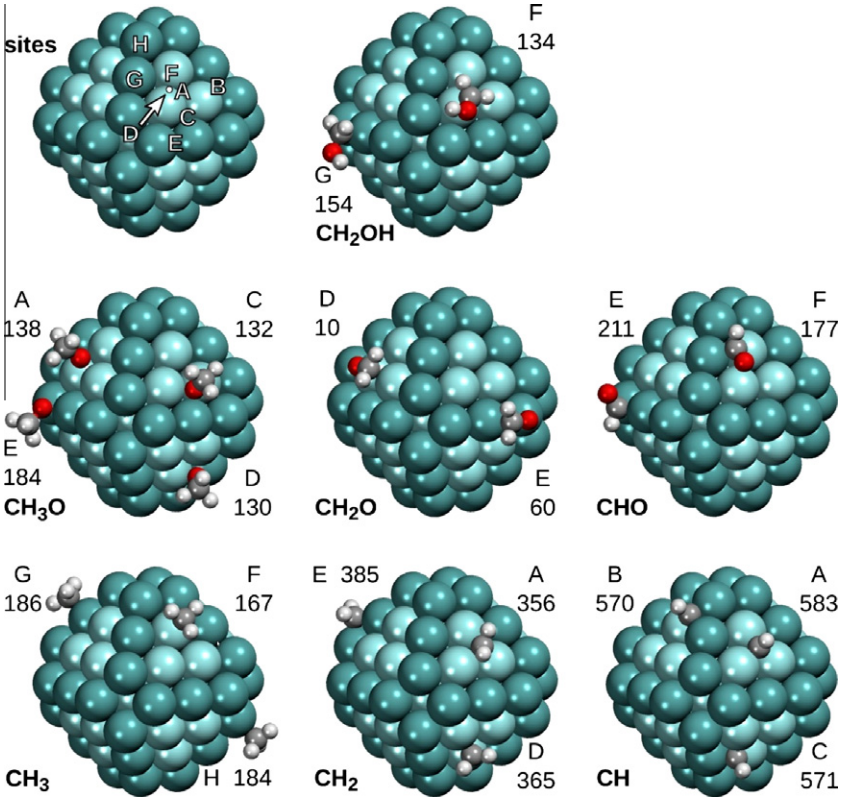

Figure 1. Calculated adsorption complexes of the CH_xO and CH_x species (x = 1–3) on various sites of Pd_{79} nanoparticle: structures and adsorption energies (in kJ/mol). See the upper left-hand side panel for the notations of the adsorption sites: **A** – μ_3 (three-fold hollow) inside a (1 1 1) facet; **B** and **C** – μ_3 on a (1 1 1) facet near edges; **D** – μ_2 inside a (1 1 1) facet; **E** – μ_2 bridging two Pd atoms of a long edge; **F** – μ_1 (on-top) inside a (1 1 1) facet; **G** – μ_1 on a Pd atom in the middle of a long edge; **H** – μ_1 on a Pd atom of a short edge. μ_i defines the bonding mode of the C atom, except for CH_3O and CHO, where the O atom is referred to. Darker large spheres – Pd atoms at the edges, lighter large spheres – Pd atoms inside the (1 1 1) facets, dark medium size spheres – C atoms, light medium size spheres – O atoms, small spheres – H atoms.

Please cite this article in press as: S.M. Kozlov et al., Chem. Phys. Lett. (2011), doi:10.1016/j.cplett.2011.02.061

formaldehyde molecule CH_2O by comparing with the experimental values [31]] (in parentheses), in cm^{-1}: asymm. stretch σ_{CH_2} – 2863 (2843), symm. stretch σ_{CH_2} – 2816 (2782), stretch $\sigma_{C=O}$ – 1758 (1746), sciss$_{CH_2}$ – 1496 (1500), rock$_{CH_2}$ – 1227 (1250), wagg$_{CH_2}$ – 1154 (1167). Only the frequencies around and above 400 cm^{-1} are listed and discussed in the following. The dipole moment of each system along the direction z perpendicular to the (1 1 1) facet interacting with the adsorbate was calculated for all displacements and used to compute intensities of the infrared (IR) vibrations as described elsewhere [32–34]. The IR spectra computed in such a way account for cancellation of the dipole moment components parallel to the nanoparticle facet under scrutiny, i.e. obey the surface selection rules.

The adsorption energy of CH_xO or CH_x adsorbate on the Pd_{79} nanoparticle, E_{ad}, is defined as the total energy difference $E_{ad} = E(Pd_{79}) + E(\text{adsorbate}) - E(\text{adsorbate}/Pd_{79})$, with adsorbate/$Pd_{79}$ being the adsorption structure. Positive E_{ad} values characterise stabilization of the adsorption structure with respect to isolated adsorbate and substrate species.

3. Results and discussion

3.1. Adsorption sites and vibrational frequencies of CH_3, CH_2 and CH on Pd_{79}

Let us start with the results for adsorption complexes of the three CH_x species, which were considered most comprehensively, i.e. employing all three approaches **1**–**3** for the atomic positions in the substrate Pd_{79} nanoparticle, as outlined in the previous section (Table 1). Some pertinent calculated geometric parameters of the adsorption complexes (also for CH_xO adsorbates) are presented in the Supplementary Information (Table S1).

In the Pd_{79} nanoparticle that was cut from the metal bulk at its experimental geometry and was kept frozen (model **1**), the Pd–Pd bond lengths are the same as on Pd surfaces; also, the small (1 1 1) facets of Pd_{79} are entirely planar similar to terraces on the Pd(1 1 1) surface. Thus, the surface sites in the interior of the (1 1 1) facets could be thought as a rather realistic representation of the corresponding sites on extended surfaces and terraces [7,17,35]. CH_3, CH_2 and CH species bind strongly to the terrace sites with adsorption energies of 155, 347 and 557 kJ/mol, respectively (Table 1). These values are slightly (by up to 3%) higher than the respective adsorption energies calculated previously on a Pd(1 1 1) slab [36]] using a functional by Becke and Perdew (BP86) [37,38]. However, for the adsorbed CH_3 and CH_2 species the (1 1 1) facets are not the most strongly bound places, whereas CH reveals quite similar binding on all studied sites, in close agreement with previous DF calculations on the Pd_{79} model [16]. Note, that the three-fold hollow terrace site **A** is a saddle point for the adsorption of CH_2 species and thus is not discussed further.

Upon relaxation of the Pd_{79} substrate (model **2**) a strengthening of the adsorption bonds is observed in most cases, by up to 12 kJ/mol for CH_3 and by 26 kJ/mol for CH. The most favourable adsorption position for CH is also changed from site **C** near the edge to site **A** in the centre of (1 1 1) nanofacet. The adsorption energy further slightly increases (by 16 kJ/mol at most) when all degrees of freedom are allowed to relax (model **3**). Thus, one can conclude that the intermediate (computationally moderately demanding) model **2** is suitable not only for the qualitatively correct DF description of the preferred adsorption sites of CH_x species on Pd particles with a diameter over 1 nm, but the energy uncertainty it introduces is quite small, around 15 kJ/mol or less. In fact, the calculations show that CH_3 strongly prefers on-top (μ_1) edge sites **G** and **H**, CH_2 is most stable on the site **E** bridging (μ_2) two Pd atoms on the edge and CH binds to three-fold hollow (μ_3) sites revealing a slight preference to the position **A** in the centre of the (1 1 1) facet. These data are in complete agreement with the finding of previous DF calculations (performed using the BP86 functional [37,38] for the energetics and localized Gaussian basis sets), where the coordination preferences of the CH_x adsorbates were rationalized in terms of the sp^3 hybridisation of the carbon atom [16].

What about vibrational frequencies of the adsorption complexes just addressed? To the best of our knowledge, there is no DF data on interactions of CH_x with nanostructured Pd. Reflection absorption IR spectroscopy (RAIRS) studies of methanol dehydrogenation on model catalysts consisting of Pd nanoparticles supported on Al_2O_3/NiAl(1 1 0) revealed two weak adsorption bands at 2945 and 2830 cm^{-1} attributed to CH_x adsorbates on Pd [39]. Even for the most studied Pd(1 1 1) surface, experimental vibrational spectroscopy data for adsorbed CH_x are scarce [40], thus preventing a detailed comparison with the calculated data listed in Table 1. We can see, that the calculated frequencies of the CH_x adsorbates are rather slightly affected by the model type **1**, **2** or **3** employed and the differences in the results from these three models hardly exceed 20–30 cm^{-1}. This means that also for computed frequencies the model **2** appears to be appropriate and only this model will be discussed in the following.

The first question is whether the computed vibrational frequencies (after a thorough calibration against the experimental frequencies of the most relevant model systems) could help in discriminating between the adsorbed CH_3, CH_2 and CH species on Pd. To this end, the following observation are pertinent: (*i*) the highest, C–H stretching frequencies at 2980–3090 cm^{-1} gradually shift along the series of the adsorbates to lower values and, obviously, the number of the C–H modes decreases with the number of the C–H bonds; (*ii*) the CH_3 species exhibits single characteristic mode around 1100 cm^{-1} together with 2 modes at 1380–1390 cm^{-1} that may be IR active or inactive depending on adsorption site (see Section 3.3); (*iii*) adsorbed CH_2 reveals a vibration at 1280–1310 cm^{-1}, which is notably lower than in the CH_3; (*iv*) finally, the highest vibrational mode of the adsorbed CH different from the C–H stretch, should appear only at 720 cm^{-1} or lower. Inspection of Table 1 shows that only for the CH_2 species, for which an asymmetric C–H stretching frequency on site **D** is by 53 cm^{-1} different from that on site **E**, one should be able to distinguish between the adsorption on terraces and edges. The vibrational frequencies of CH on terrace site **A** are systematically higher by 20–30 cm^{-1} than those on sites **B** and **C** closer to the edge; however, the difference is comparable with accuracy of our calculations. Finally, the frequencies of the CH_3 species that are above 1000 cm^{-1}, vary only slightly from one adsorption site to the other, by less than 10 cm^{-1}. However, if the considerations of the IR intensity change depending on the adsorption site are invoked (see Section 3.3) more information practically useful for the characterization of the adsorption complexes could be extracted from the calculated data.

3.2. Adsorption and vibrational frequencies of CH_2OH, CH_3O, CH_2O and CHO on Pd_{79}

The results of calculations for the adsorption complexes CH_xO/Pd_{79} are shown in Figure 1 and Table 2; the geometrical characteristics of the calculated structures are listed in Table S1 in Supplementary Materials. Hydroxymethyl, CH_2OH, is 20 kJ/mol more stable on the edge on-top site **G** of Pd_{79} than at site **F** inside the (1 1 1) facet. The preference of methoxy, CH_3O, to occupy an edge μ_2 site **E** with respect to the μ_2 **A** and **C** and μ_3 **D** sites of Pd_{79} is even stronger, by about 50 kJ/mol. Formaldehyde, CH_2O, binds to (1 1 1) facets of Pd_{79} (μ_2 site **D**) weakly, with the adsorption energy of only 10 kJ/mol, in line with the observations for the Pd(1 1 1) surface [9,40]. The adsorption is notably stronger, 60 kJ/mol, on

Table 1
Calculated adsorption energies E_{ads} and harmonic vibrational frequencies ω of the optimised CH_x species adsorbed on various sites of a Pd_{79} nanoparticle (see Figure 1). Italic font – Pd atoms are kept fixed at the experimental positions in Pd bulk (approach **1**, see text); straight font – Pd atoms are kept fixed at the optimised positions of bare Pd_{79} (approach **2**, gray background); in parentheses – fully optimised structures CH_x/Pd_{79} (approach **3**). Assignment of the vibrations is also given for the most stable structures.[a]

Adsorbate	Site	E_{ads} kJ/mol	ω cm^{-1}								
CH_3	**F**	*155*	*3084*	*3075*	*2974*	*1385*	*1383*	*1091*	*658*	*649*	*432*
		167	3085	3080	2977	1388	1383	1096	660	657	448
		(178)	(3090)	(3087)	(2981)	(1390)	(1384)	(1100)	(671)	(664)	(472)
	G	*182*	*3090*	*3069*	*2971*	*1398*	*1382*	*1101*	*651*	*633*	*459*
		186	3094	3076	2977	1397	1384	1101	656	639	457
		(190)	(3095)	(3079)	(2977)	(1398)	(1383)	(1102)	(656)	(646)	(467)
	H	*183*	*3096*	*3076*	*2974*	*1392*	*1390*	*1101*	*644*	*630*	*466*
		184	3094	3076	2973	1392	1391	1102	648	631	463
		(187)	(3097)	(3075)	(2972)	(1390)	(1390)	(1104)	(646)	(632)	(469)
			σ_{CH_3}	σ_{CH_3}	σ_{CH_3}	def	def	umbr	δ	δ	σ_{Pd}
CH_2	**A**[b]	*316*	*2997*	*2921*	*1311*	*800*	*573*	*505*	*501*	*376*	
		356	2910	2869	1291	749	511	449	355	316	
		(345)	(3027)	(2945)	(1312)	(830)	(612)	(546)	(531)	(412)	
	D	*347*	*3008*	*2934*	*1307*	*794*	*570*	*505*	*489*	*377*	
		365	3012	2937	1308	807	585	528	500	392	
		(377)	(3039)	(2956)	(1309)	(821)	(608)	(532)	(530)	(405)	
	E	*386*	*3061*	*2964*	*1289*	*791*	*595*	*544*	*520*	*425*	
		385	3065	2967	1286	795	601	552	527	413	
		(393)	(3060)	(2963)	(1289)	(811)	(602)	(556)	(533)	(417)	
			σ_{CH_2}	σ_{CH_2}	sciss	wagg	rock	σ_{Pd}	twist	σ_{Pd}	
CH	**A**	*557*	*3008*	*720*	*718*	*576*	*461*	*458*			
		583	3010	720	716	603	471	467			
		(599)	(3042)	(706)	(704)	(587)	(473)	(471)			
	B	*564*	*2985*	*710*	*691*	*573*	*465*	*444*			
		570	2984	702	688	577	460	443			
		(584)	*(2961)*	*(709)*	*(693)*	*(555)*	*(483)*	*(451)*			
	C	*561*	*2995*	*721*	*719*	*573*	*467*	*457*			
		571	2988	717	713	576	459	453			
		(585)	(2973)	(739)	(734)	(546)	(491)	(469)			
			σ_{CH}	δ	δ	σ_{Pd}	σ_{Pd}	σ_{Pd}			

[b] **A** is a saddle point structure for the diffusion of CH_2 on Pd_{79}.

[a] σ_{CHx} – C–H stretching (in all cases asymmetric vibrations have higher frequencies than the symmetric one); σ_{Pd} – Pd–C stretching; δ – bending with respect to the substrate; def – deformation of CH_3; umbr – umbrella mode of CH_3; sciss, wagg, rock, twist – scissor, wagging, rocking and twisting vibrations of CH_2, respectively.

Table 2
Calculated adsorption energies E_{ads} and harmonic vibrational frequencies ω of the adsorbed CH_xO species optimised on various sites of a bare Pd_{79} nanoparticle (model **2**, see Table 1, Figure 1). Assignments of the vibrations are also given for the most stable structures.[a]

Adsorbate	Site	E_{ads} kJ/mol	ω cm^{-1}									
CH_2OH	**F**	134	3654	3092	2986	1426	1330	1135	1070	962	685	458
	G	154	3700	3063	2958	1428	1333	1132	1069	1003	673	460
			σ_{OH}	σ_{CH_2}	σ_{CH_2}	sciss	δ_{OCH}	σ_{CO}	δ_{OCH}	wagg	σ_{Pd}	σ_{Pd}
CH_3O	**A**	138	3015	3013	2936	1441	1441	1413	1110	1108	977	
	C	132	3022	3016	2940	1443	1436	1413	1101	1098	966	
	D	130	3023	3006	2932	1439	1438	1410	1108	1099	962	
	E[b]	184	3012	2999	2927	1450	1437	1412	1128	1115	986	
			σ_{CH_3}	σ_{CH_3}	σ_{CH_3}	umbr	def	def	σ_{CO}	δ_{OCH}	δ_{OCH}	
CH_2O	**D**	10	2929	2851	1452	1231	1147	918	516	415		
	E	60	2944	2865	1444	1235	1151	929	490	429		
			σ_{CH_2}	σ_{CH_2}	σ_{CO}	sciss	rock	wagg	σ_{Pd}	σ_{Pd}		
CHO	**E**[b]	211	2755	1584	1090	591	398					
	F[c]	177	2855	1376	1123	670	449					
			σ_{CH}	σ_{CO}	δ_{OCH}	σ_{Pd}	σ_{Pd}					

[a] σ_{OH} – O–H stretching; σ_{CHx} – C–H stretching (in all cases asymmetric vibrations have higher frequencies than the symmetric one); σ_{Pd} – Pd–C or Pd–O stretching; δ_{ABC} – bending of A–B–C bonds; def – deformation of CH_3; umbr – umbrella mode of CH_3; sciss, wagg, rock – scissor, wagging and rocking vibration modes of CH_2, respectively.

[b] CH_3O and CHO spontaneously move from site **B** to site **E** during geometry optimisation.

[c] CHO is adsorbed in μ_1–μ_2 fashion on the site **F** with O coordinated by one Pd atom and C by two Pd atoms.

the edge μ_2 site **E**. This considerable increase in the binding strength of formaldehyde through an interaction with low-coordinated Pd atoms of Pd_{79} is in accord with the findings of earlier DF studies on stepped extended surfaces [41,42] as well as on sub-nanometer Pd clusters [43]. Thus, nanostructuring of Pd surfaces stabilizing adsorbed formaldehyde is also expected to dramatically affect its reactivity under specific conditions. The formyl species CHO reveals rather strong adsorption interactions,

but its most stable position on Pd_{79} with the adsorption energy 211 kJ/mol is a μ_2 site **E** bridging two edge Pd atoms. Thus, all the CH_xO adsorbates under consideration show a strong propensity to be located at the edges of Pd nanoparticles, which implies a considerably different reactivity on nanostructured Pd versus that on single crystal surfaces when the CH_xO species take part in the reactions. Note that calculations on CH_xO species adsorbed at (1 1 1) facets of the Pd_{79} nanoparticle performed using another common gradient-corrected exchange–correlation functional BP86 [37,38] revealed systematically higher (by up to 15%) adsorption energies [16].

The following IR spectroscopy data are available in the literature for the CH_xO/Pd(1 1 1) adsorption complexes: trace amounts of methoxy (CH_3O) are detected at 2900 cm^{-1}; formaldehyde (CH_2O) manifests itself by the modes at 1305 and 1255 cm^{-1} assigned to two different adsorption geometries; formyl (CHO) reveals a peak at 1200 cm^{-1}, which is either bending δ_{OCH} or stretching σ_{CO} mode [12,40]. On a model catalyst $Pd/Al_2O_3/NiAl(1\ 1\ 0)$ two RAIRS shoulders at 2905 and 2800 cm^{-1} are tentatively assigned to methoxy species adsorbed on Pd nanoparticles [39]. Missing spectroscopic indications of any intermediates of methoxy dehydrogenation on the model catalyst imply that the subsequent decomposition steps are fast [44]. The calculated vibrational frequencies of CH_xO/Pd_{79} in Table 2 show (*i*) that similarly to the CH_x/Pd_{79} systems (see Section 3.1), some of the discussed species exhibit a pronounced change in vibrational frequencies at different adsorption sites, e.g. CH_2OH and CHO, while others show no change in frequencies, e.g. CH_3O and CH_2O; (*ii*) there is a quite substantial systematic frequency shift of the highest stretching mode to lower values in the series of adsorbed CH_2OH (3700 cm^{-1}, O–H stretch) > CH_3O (3012 cm^{-1}, O–H stretch) > CH_2O (2944 cm^{-1}, O–H stretch) > CHO (2755 cm^{-1}, O–H stretch). There are also other less pronounced trends in the calculated frequencies, which could be used for characterization of the species. Additional useful information comes from the analysis of the IR intensities computed for selected surface complexes and discussed in the following section.

3.3. Positions of the adsorbates and IR intensities

Before closing the discussion, let us briefly comment how IR intensities may give indication about the preferred adsorption positions of certain species. Most of the studied CH_xO and CH_x species orient differently orientations with respect to a (1 1 1) facet when adsorbed on the sites inside the facet and at an edge of the corresponding (1 1 1) facet of Pd_{79} nanoparticle (Figure 1). In turn, (1 1 1) facets of larger transition metal nanoparticles prepared by deposition on conducting oxide films are often parallel to the substrate plane [39]. Thus, C_1 species adsorbed on the terraces and at the edges of the nanoparticles may reveal substantially different peak intensities in their IR spectra due to electrostatic interactions with the substrate. Vibrations that do not manifest themselves in the IR spectra of the species adsorbed on terraces due to surface selection rules may become visible when the molecule is adsorbed at an edge. And vice versa, the intensities of vibrations normal to (1 1 1) facets may be decreased or even reduced to zero. Indeed, Figure 2 illustrates these considerations for selected adsorbates at selected positions.

For example, the CH_2 scissor mode of CH_2OH at ~1430 cm^{-1} should be visible in the IR spectra (provided that the species does not decompose) only in the case of adsorption at an edge (site **G**). In contrast, the C–O–H bending mode at ~1330 cm^{-1} should be IR-visible only when CH_2OH is adsorbed at a nanoparticle terrace (site **F**). This implies that adsorption at sites **G** and **F**, energetically apart by only 20 kJ/mol, could be distinguishable via a strong intensity alteration of the IR peaks separated by ~100 cm^{-1} and thus be eventually detectable.

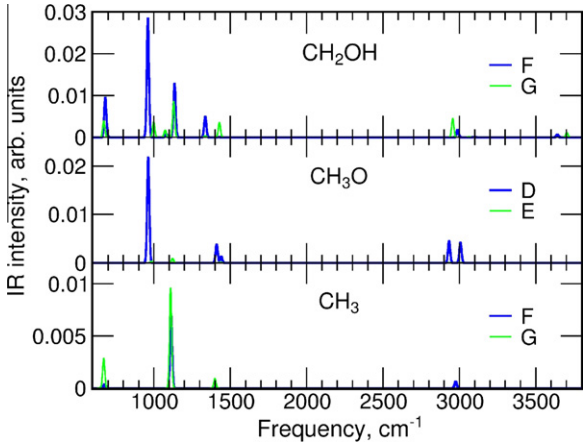

Figure 2. Calculated IR spectra for adsorption complexes of CH_2OH, CH_3O and CH_3 on selected sites of the optimised Pd_{79} nanoparticle. See Figure 1 for the definition of the sites.

Likewise, the adsorbed CH_3 and CH_3O species have three vibrational modes associated with the stretching of C–H bonds. However, not all of these modes are always visible in the IR spectra due to their different symmetry. Whereas on the (1 1 1) terrace (site **F**) only a symmetric stretch of three C–H bonds in CH_3 is IR-active, in the case of adsorption at an edge (site **G**) there is also another IR peak at a higher frequency, associated with the asymmetric CH_3 stretching. In this case, a peak that appears near 1400 cm^{-1} is caused by an asymmetric bending of the C–H bonds.

The CH_3O species adsorbed on a (1 1 1) terrace of Pd nanoparticle are tilted, so that the symmetric and one of asymmetric modes are IR-visible. However, when CH_3O is adsorbed on the edge of nanoparticle (the notably preferred site **E**) the CH_3 group is oriented nearly perpendicularly to one of (1 1 1) facets, resulting in the negligible IR intensities of the CH_3 vibrations in the frequency regions around 3000 cm^{-1} and 1400 cm^{-1} (Figure 2). Thus, also for the methoxide adsorbate its spectroscopic detection and characterisation on Pd nanoparticles could be facilitated with the help of our computationally predicted IR intensity features.

4. Summary

The main results of this study can be summarized as follows:

- All studied C_1 adsorbates except CH are computed to be stabilized on the edge sites of the nanoparticle Pd_{79} with respect to the sites in the interior of the (1 1 1) facets, the latter serve in our models to represent Pd(1 1 1) terraces. The stabilization is quite significant, 20–50 kJ/mol, which implies a notable effect of low-coordinated atoms exposed by Pd catalyst particles on the thermodynamics and kinetics of the processes involving the C_1 species as reactants, intermediates or products. The largest stabilization on edges is observed for formaldehyde, whose adsorption energy increases from 10 kJ/mol on terraces to 60 kJ/mol on edges.
- Some of the studied species do not show a significant dependence of their vibrational frequencies on the adsorption site (~15 cm^{-1} for CH_3O, CH_2O, CH_3) whereas the frequencies of several other adsorbates (CH_2OH, CHO, CH_2, CH) do change by 30 cm^{-1} or more. The frequency variations appear to be rather modest compared to the pronounced changes in the adsorption energies and structural changes at different adsorption sites.
- The spatial orientations of various C_1 species adsorbed on nanoparticle edges are changed with respect to adsorption on flat terraces, yielding pronounced changes in the IR intensities.

Vibrations that cannot be observed on extended surfaces due to the surface selection rule could manifest themselves in the IR spectra taken on nanoparticles, while the intensities of other IR peaks detectable on flat surfaces may be dramatically reduced. These findings together with the frequency shifts associated with the adsorption on nanoparticle edges may help to characterise usually elusive C_1 adsorption species formed and disappearing rapidly in pertinent reactions on Pd catalysts.

Acknowledgements

SMK is grateful to the Spanish *Ministerio de Educación* for a predoctoral FPU grant. GFC thanks CONICET and ANPCyT (PICT N° 02419) of Argentina for financing her stay in Barcelona. Financial support has been provided by Spanish MICINN (grants FIS2008-02238) and by *Generalitat de Catalunya* (grants 2009SGR1041 and XRQTC). Computational time on MARENOSTRUM supercomputer granted by the Barcelona Supercomputing Center is also acknowledged.

Appendix A. Supplementary data

Supplementary data associated with this article can be found, in the online version, at doi:10.1016/j.cplett.2011.02.061.

References

[1] G. Ertl, Reactions at Solid Surfaces, second ed., J. Wiley, Hoboken, 2009. p. 208.
[2] M. Bowker, ACS Nano 1 (2007) 253.
[3] H.-P. Steinrück, J. Libuda, D.A. King, Chem. Soc. Rev. 37 (2008) 2152.
[4] R. Imbihl, R.J. Behm, R. Schlögl, Phys. Chem. Chem. Phys. 9 (2007) 3459.
[5] M. Bäumer, H.-J. Freund, Prog. Surf. Sci. 61 (1999) 127.
[6] H.-J. Freund, Chem. Eur. J. 16 (2010) 9384.
[7] I.V. Yudanov, R. Sahnoun, K.M. Neyman, N. Rösch, J. Chem. Phys. 117 (2002) 9887.
[8] K.M. Neyman, F. Illas, Catal. Today 105 (2005) 2.
[9] M. Bäumer, J. Libuda, K.M. Neyman, N. Rösch, G. Rupprechter, H.-J. Freund, Phys. Chem. Chem. Phys. 9 (2007) 3541.
[10] T. Fuhrmann, M. Kinne, B. Tränkenschuh, C. Papp, J.F. Zhu, R. Denecke, H.-P. Steinrück, New J. Phys. 7 (2005) 107.
[11] F. Zaera, Prog. Surf. Sci. 69 (2001) 1.
[12] G. Rupprechter, C. Weilach, J. Phys.: Condens. Matter 20 (2008) 184019.
[13] A.J. Foster, R.F. Lobo, Chem. Soc. Rev. 39 (2010) 4783.
[14] I.V. Yudanov et al., J. Phys. Chem. B 107 (2003) 255.
[15] I.V. Yudanov, K.M. Neyman, N. Rösch, Phys. Chem. Chem. Phys. 8 (2006) 2396.
[16] I.V. Yudanov, A.V. Matveev, K.M. Neyman, N. Rösch, J. Am. Chem. Soc. 130 (2008) 9342.
[17] F. Viñes, A. Desikusumastuti, T. Staudt, A. Görling, J. Libuda, K.M. Neyman, J. Phys. Chem. C 112 (2008) 16539.
[18] F. Viñes, C. Loschen, F. Illas, K.M. Neyman, J. Catal. 266 (2009) 59.
[19] F. Viñes et al., Chem. Eur. J. 16 (2010) 6530.
[20] K.M. Neyman, S. Schauermann, Angew. Chem. Int. Edit. 49 (2010) 4743.
[21] Z.-J. Zhao, L.V. Moskaleva, H.A. Aleksandrov, D. Basaran, N. Rösch, J. Phys. Chem. C 114 (2010) 12190.
[22] G. Kresse, J. Furthmuller, Phys. Rev. B 54 (1996) 11169.
[23] G. Kresse, J. Hafner, Phys. Rev. B 47 (1993) 558.
[24] G. Kresse, D. Joubert, Phys. Rev. B 59 (1999) 1758.
[25] B. Hammer, L.B. Hansen, J.K. Nørskov, Phys. Rev. B 59 (1999) 7413.
[26] F. Viñes, F. Illas, K.M. Neyman, J. Phys. Chem. A 112 (2008) 8911.
[27] F. Baletto, R. Ferrando, Rev. Mod. Phys. 77 (2005) 371.
[28] S.T. Bromley, I. de P.R. Moreira, K.M. Neyman, F. Illas, Chem. Soc. Rev. 38 (2009) 2657.
[29] F. Viñes, F. Illas, K.M. Neyman, Angew. Chem. Int. Ed. 46 (2007) 7094.
[30] G. Herzberg, Molecular Spectra and Molecular Structure: II. Infrared and Raman Spectra of Polyatomic Molecules, Krieger, Malabar, 1991.
[31] R.J. Bouwens, J.A. Hammerschmidt, M.M. Grzeskowiak, T.A. Stegnik, P.M. Yorba, W.F. Polik, J. Chem. Phys. 104 (1996) 460.
[32] R.D. Amos, Adv. Chem. Phys. 67 (1987) 99.
[33] K.M. Neyman, N. Rösch, Ber. Bunsenges. Phys. Chem. 96 (1992) 1711.
[34] A. Valcárcel, J.M. Ricart, F. Illas, A. Clotet, J. Phys. Chem. B 108 (2004) 18297.
[35] I.V. Yudanov, M. Metzner, A. Genest, N. Rösch, J. Phys. Chem. C 112 (2008) 20269.
[36] J.-F. Paul, P. Sautet, J. Phys. Chem. B 102 (1998) 1578.
[37] A.D. Becke, Phys. Rev. A 38 (1988) 3098.
[38] J.P. Perdew, Phys. Rev. B 33 (1986) 8822.
[39] S. Schauermann, J. Hoffmann, V. Johánek, J. Hartmann, J. Libuda, Phys. Chem. Chem. Phys. 4 (2002) 3909.
[40] M. Borasio, O. Rodríguez de la Fuente, G. Rupprechter, H.-J. Freund, J. Phys. Chem. B 109 (2005) 17791.
[41] Z.-X. Chen, K.H. Lim, K.M. Neyman, N. Rösch, J. Phys. Chem. B 109 (2005) 4568.
[42] K.H. Lim, Z.-X. Chen, K.M. Neyman, N. Rösch, J. Phys. Chem. B 110 (2006) 14890.
[43] F. Mehmood, J. Greeley, L.A. Curtiss, J. Phys. Chem. C 113 (2009) 21789.
[44] S. Bertarione et al., J. Catal. 223 (2004) 64.